JGR Space Physics

RESEARCH ARTICLE
10.1029/2021JA029708

Scale Factors of the Thermospheric Density: A Comparison of Satellite Laser Ranging and Accelerometer Solutions

Lea Zeitler[1], Armin Corbin[2], Kristin Vielberg[2], Sergei Rudenko[1], Anno Löcher[2], Mathis Bloßfeld[1], Michael Schmidt[1], and Jürgen Kusche[2]

[1]Deutsches Geodätisches Forschungsinstitut, Technische Universität München, Munich, Germany, [2]Institute of Geodesy and Geoinformation, University of Bonn, Bonn, Germany

Key Points:

- For the first time, we compare scale factors of the thermospheric density derived from satellite laser ranging (SLR) and accelerometer measurements
- The estimated scale factors vary by up to 30% at low solar activity and up to 70% at high solar activity from the desired value 1
- Correlations of 0.7–0.8 are obtained between the estimated scale factors from SLR and accelerometer measurements depending on the height

Correspondence to:

L. Zeitler,
lea.zeitler@tum.de

Citation:

Zeitler, L., Corbin, A., Vielberg, K., Rudenko, S., Löcher, A., Bloßfeld, M., et al. (2021). Scale factors of the thermospheric density: A comparison of satellite laser ranging and accelerometer solutions. *Journal of Geophysical Research: Space Physics*, *126*, e2021JA029708. https://doi.org/10.1029/2021JA029708

Received 23 JUN 2021
Accepted 30 NOV 2021

Abstract A major problem in the precise orbit determination (POD) of satellites at altitudes below 1,000 km is the modeling of the aerodynamic drag which mainly depends on the thermospheric density and causes the largest non-gravitational acceleration. Typically, empirical thermosphere models are used to calculate density values at satellite positions but current thermosphere models cannot provide the required accuracy. Thus, unaccounted variations in the thermospheric density may lead to significantly incorrect satellite positions. For the first time, we bring together thermospheric density corrections for the NRLMSISE-00 model in terms of scale factors with a temporal resolution of 12 hr derived from satellite laser ranging (SLR) and accelerometer measurements. Whereas, the latter are *in situ* information given along the satellite orbit, SLR results have to be interpreted as mean values along the orbit within the underlying time interval. From their comparison, we notice a rather similar behavior with correlations of up to 80% and more depending on altitude. During high solar activity, scale factors vary around 30% at low solar activity and up to 70% at high solar activity from the value one. In addition, we found the scaled thermospheric density decreasing stronger as the modeled density of NRLMSISE-00. To check the reliability of the SLR-derived scale factors, we compare the POD result of two different software packages, namely DOGS-OC from DGFI-TUM and GROOPS from IGG Bonn. Furthermore, a validation of our estimated scale factors with respect to an external data set proofs the high quality of the obtained results.

Plain Language Summary Variations in the density of the thermosphere must be taken into account when modeling and predicting the motion of satellites in the near-Earth environment. Typically, thermospheric densities at the position of satellites are provided by models, but their accuracy is limited. Due to the sensitivity of satellites orbiting the Earth in the altitude range of the thermosphere, they can be used to derive information about the thermospheric density. In this study, we compare for the first time thermospheric density corrections in terms of scale factors for the NRLMSISE-00 model with a temporal resolution of 12 hr derived from two geodetic measurement techniques, namely satellite laser ranging (SLR) and accelerometry. Our results demonstrate that both measurement techniques can be used to derive comparable scale factors of the thermospheric density, which vary around the desired value one. This indicates to which extent the NRLMSISE-00 model differs from the observed thermospheric density. On average, during high solar activity, the model underestimates the thermospheric density and can be scaled up using the estimated scale factors. We additionally discuss our estimated scale factors with respect to an external data set. Furthermore, we validate the approach of deriving scale factors from SLR measurements by using two independent software packages.

1. Introduction

Even today, modeling the non-gravitational accelerations acting on low Earth orbiting (LEO) satellites with altitudes lower than 1,000 km is a great challenge. Among them, the aerodynamic drag mainly depending on the density of the thermosphere is the largest. For example, a mis-modeling in the density of 5% may lead to a position error of more than 100 m after 7 days in the precise orbit determination (POD) of a spherical LEO satellite at a mean altitude of 680 km. Consequently, the knowledge of the thermospheric density is of crucial importance for POD, but also for re-entry prediction, maneuver planning, and satellite lifetime planning, as well as for many geo-scientific applications such as remote sensing, satellite gravity missions and satellite altimetry. In the latter case, for example, for sea level studies, the satellite orbits need to be known with an accuracy of a few millimeters, see for example, Rudenko et al. (2017).

In the past, various thermosphere models have been developed. As output parameters they comprise amongst others the density and the temperature by taking into account the complex interactions between the atmosphere and the solar as well as the geomagnetic activity. In general, thermosphere models can be categorized into empirical and physical ones. Examples of empirical models are the NRLMSISE-00 model (Picone et al., 2002), its follow-up, the NRLMSIS 2.0 model (Emmert, Drob, et al., 2021), the Jacchia-Bowman 2008 model (JB2008; Bowman et al., 2008), the Drag Temperature Model 2013 (DTM2013; Bruinsma, 2015), and the CH-Therm2018 model (Xiong et al., 2018). For the second type of models, the consideration of the physical coupling processes between the neutral thermosphere and the charged ionosphere is fundamental. An example of such a model is the Thermosphere-Ionosphere-Electrodynamics General Circulation Model (TIE-GCM) developed by the National Center of Atmospheric Research (NCAR). It provides a comprehensive, three-dimensional, non-linear representation of the coupled thermosphere and ionosphere system (Qian et al., 2014). All the aforementioned models are based on slightly different input data sets and thus, may lead to rather different results, in particular in case of strong space weather events. As input data sets, we want to mention globally defined solar and geomagnetic indices, for example, the F10.7 solar index (Tapping, 2013), the 30-cm solar flux index (De Wit & Bruinsma, 2017), the Mg II core-to-wing solar index (Viereck & Puga, 1999), as well as the geomagnetic Kp and ap indices (Bartels et al., 1939; Matzka et al., 2021).

Due to the sensitivity of LEO satellites, an appropriate satellite on-board instrumentation (accelerometer, tracking equipment, reflectors, and so forth) can be used to derive information about the thermospheric density. Therefore, the aforementioned thermosphere models can be improved by ingesting observations, for example, from geodetic measurement techniques. To account for possible inconsistencies in the modeled thermospheric density scale factors can be considered; see for example, Lean et al. (2006), Doornbos (2012), or Panzetta et al. (2018). In this study, we juxtapose scale factors derived from satellite laser ranging (SLR) and accelerometer measurements to investigate their comparability; that is, we assume to obtain the same corrections with respect to the modeled thermospheric density by applying two different measurement procedures to satellites of different shape orbiting the Earth at different altitudes. In the last decade, accelerometers, for example, on CHAMP (CHAllenging Minisatellite Payload) and GRACE (Gravity Recovery And Climate Experiment), have become more and more important for providing thermosphere data with unprecedented accuracy and resolution (Mehta et al., 2017). In addition to the density, these measurements also enable the derivation of wind data sets, for example, Sutton et al. (2007) and Doornbos et al. (2010). Accelerometer measurements are in-situ observations of very high temporal resolution, but only given along the satellite orbit.

Since satellites above 550 km are usually not equipped with accelerometers, SLR measurements to satellites flying at similar but also higher altitudes can act as a suitable complement to provide information on the thermospheric density. The main advantage of the SLR technique is its use for the POD of a variety of satellites equipped with retro-reflectors orbiting the Earth at mean altitudes below 1,000 km, where the accuracy and temporal resolution is higher than, for example, for two-line element (TLE) derived data (Doornbos, 2012). The SLR observation technique is based on the precise measurement of the two-way travel time of laser pulses emitted from a ground station to a satellite equipped with retro-reflectors, typically achieving a normal point precision of 0.25–1.2 cm (Pearlman et al., 2019). Thus, SLR observations are very sensitive to any perturbing acceleration acting on a satellite.

The SLR tracking priority list includes a large number of satellites and is organized by the International Laser Ranging Service (ILRS; Pearlman et al., 2019). Since SLR is, unfortunately, restricted to a limited number of inhomogeneously distributed ground stations, it suffers from a rather sparse observation coverage.

Whereas accelerometer measurements provide *in-situ* information along the satellite orbit, SLR allows for the determination of information integrated along the satellite orbit over a given time interval of several hours. Consequently, in this study, we compare and discuss for the first time the results for the thermospheric density scale factors estimated from SLR and accelerometer measurements. For that purpose, we take into account both the completely different measurement principles and the estimation procedures. Since we possess two extensive POD software packages, we additionally compare the estimated scale factors from the two packages for selected spherical satellites. In this comparison, we take further advantage of the long mission lifetimes of the selected satellites, which allow us to study scale factor time series over more than 30 years (1989–2020), that is, almost three solar cycles.

In the following Section 2, the theoretical background of thermospheric drag modeling is presented briefly. The procedures for the estimation of thermospheric density scale factors from SLR measurements—including the two independent SLR POD software packages—and accelerometer measurements are presented in Section 3. After comparing, analyzing and interpreting the results in Section 4, the conclusions and an outlook on future work are drawn in the final Section 5.

2. Theoretical Background

The equation of motion of a satellite, that is, its total acceleration or the second derivative of the satellite's position vector $\mathbf{r}_{sat}(t)$ with respect to time t,

$$\frac{d^2\mathbf{r}_{sat}(t)}{dt^2} = \mathbf{a}_{sat} = \mathbf{a}_G + \mathbf{a}_{NG} \tag{1}$$

can be expressed as the sum of the gravitational acceleration $\mathbf{a}_G$–consisting of a direct and an indirect part—and the non-gravitational acceleration,

$$\mathbf{a}_{NG} = \mathbf{a}_{aero} + \mathbf{a}_{srp} + \mathbf{a}_{erp} + \mathbf{a}_{others}, \tag{2}$$

see Montenbruck and Gill (2000). More precisely, $\mathbf{a}_{NG}$ consists of the aerodynamic acceleration $\mathbf{a}_{aero}$, the acceleration $\mathbf{a}_{srp}$ due to solar radiation pressure (SRP), the acceleration $\mathbf{a}_{erp}$ due to Earth albedo and Earth infrared radiation pressure (ERP), as well as other kinds of accelerations $\mathbf{a}_{others}$, such as the radiation pressure of the Moon, see, for example, Doornbos (2012). The aerodynamic acceleration reads

$$\mathbf{a}_{aero} = -\frac{1}{2}\,\frac{A_{ref}}{m}\,\mathbf{c}_{aero}\,\rho_M\,v_{rel}^2, \tag{3}$$

where $\mathbf{c}_{aero}$ is a dimensionless force coefficient vector depending on the geometry and orientation of the satellite, A_{ref} is the effective cross-section of the satellite interacting with the atmosphere, m means the total satellite mass, ρ_M is the thermospheric density and $v_{rel} = |\mathbf{v}_{rel}|$ means the velocity of the satellite relative to the atmosphere (Doornbos, 2012). The relative velocity vector $\mathbf{v}_{rel}$ is defined as the sum

$$\mathbf{v}_{rel} = \mathbf{v}_{r,i} + \mathbf{v}_{r,c} + \mathbf{v}_{r,w} \tag{4}$$

of the inertial velocity vector $\mathbf{v}_{r,i}$ of the satellite along its orbit, the velocity vector $\mathbf{v}_{r,c}$ caused by the rotation of the atmosphere and the velocity vector $\mathbf{v}_{r,w}$ caused by winds in the atmosphere. Introducing the unit vector $\mathbf{x} = \mathbf{v}_{r,i}/|\mathbf{v}_{r,i}|$ pointing into the direction of $\mathbf{v}_{r,i}$, we obtain the along track component of the aerodynamic acceleration by the scalar product $\mathbf{x}^T\mathbf{a}_{aero}$.

As mentioned before, we estimate in our study scale factors for the thermospheric density from SLR and accelerometer measurements. Consequently, we distinguish in the sequel between the

1. Approach: Utilization of the POD of LEO satellites to estimate scale factors of the thermospheric density from SLR tracking measurements, and the
2. Approach: Calculation of scale factors of the thermospheric density from evaluating the aerodynamic acceleration using satellite accelerometer measurements

The first approach is typically applied to spherical satellites, where the perpendicular component of the aerodynamic acceleration can be neglected, since it has much less influence on the orbit than the along-track acceleration component $\mathbf{x}^T\mathbf{a}_{aero}$. Furthermore, the attitude of the satellite does not have to be modeled since the cross-sectional area A_{ref} remains constant. Therefore, we assume in case of spherical LEO satellites $\mathbf{a}_{aero} \approx \mathbf{a}_D$ and obtain from Equation 3

$$\mathbf{a}_D = -\frac{1}{2}\,\frac{A_{ref}}{m}\,C_D\,\rho_M\,v_{rel}^2\,\mathbf{x}. \tag{5}$$

The drag acceleration (5) is a velocity-dependent non-conservative perturbation, where C_D means a dimensionless aerodynamic drag coefficient describing the interaction of the atmosphere with the satellite surface; for more details concerning Equation 5 see, for example, Doornbos (2012) or Panzetta et al. (2018). In this study, we apply

the first approach to the four spherical LEO satellites Starlette, WESTPAC, Stella and Larets orbiting the Earth at different altitudes; more details will be given in Section 3.1 and in Figure 2.

When calculating thermospheric densities according to the second approach from an accelerometer on-board nonspherical satellites, we have to deal with two challenges, namely (1) the geometry and attitude of the complex-shaped satellite surface and (2) its interaction with the atmospheric particles. In opposite to the first approach based on spherical satellites, we have to consider here the perpendicular component of the aerodynamic acceleration, that is, the side and lift effects. In other words, the second approach requires the availability and the use of a high-quality macro model of the chosen satellite for the evaluation of Equation 3. Furthermore, the attitude realization is important since it significantly influences A_{ref}. Here, a nominal or an observation-based attitude realization can be used; see for example, Bloßfeld et al. (2020). According to the direct processing algorithm described by Doornbos (2012), the observed drag acceleration from accelerometer measurements can be determined. In this study, the utilization and evaluation of accelerometer data from the LEO satellite missions CHAMP and GRACE is discussed in detail in Section 3.2.

3. Estimation of Thermospheric Density Scale Factors

3.1. Satellite Laser Ranging (SLR)

SLR provides highly accurate (sub cm-level) travel time measurements of laser pulses reflected at retro-reflectors mounted on satellites, which have been emitted from globally distributed telescopes located at the Earth's surface. This technique can also be used to determine various geodetic parameters such as the position and velocity vector of reference points at tracking stations, Earth rotation parameters, and Earth gravity field coefficients (Bloßfeld et al., 2018).

Following the first approach introduced in Section 2, we formulate the observation equation of the SLR one-way range measurement p and its error e_{p} averaged from the two way travel time as

$$p + e_{\text{p}} = \|\mathbf{r}_{\text{sat}}(t_{\text{M}} + \Delta t) - \mathbf{r}_{\text{sta}}(t_{\text{M}} + \Delta t)\| + \Delta p, \tag{6}$$

where we consider on the right-hand side, for simplification, only the geometrical distance $\|\mathbf{r}_{\text{sat}}(t_{\text{M}} + \Delta t) - \mathbf{r}_{\text{sta}}(t_{\text{M}} + \Delta t)\|$ and a range bias Δp; a more detailed version of the observation equation is provided, for example, by Bloßfeld (2015) or Panzetta et al. (2018). In Equation 6, $\mathbf{r}_{\text{sat}}$ means according to Equation 1 the position vector of the satellite's center of mass in the Geocentric Celestial Reference System (GCRS), t_{M} is the time epoch of reflection of the laser pulse at the satellite, Δt is the time bias of the measurement, and $\mathbf{r}_{\text{sta}}$ is the position vector of the station converted from the International Terrestrial Reference System (ITRS; Petit & Luzum, 2010) to the GCRS using Earth orientation parameters.

Since we want to estimate scale factors from SLR analyses, we extend the right-hand side of Equation 5 by the time-dependent scale factor $f_{\text{s,SLR}} = f_{\text{s,SLR}}(t)$, such that the modified drag acceleration reads

$$\mathbf{a}_{\text{D}} = -\frac{1}{2}\, f_{\text{s,SLR}}\, \frac{A_{\text{ref}}}{m}\, C_{\text{D}}\, \rho_{\text{M}}\, v_{\text{rel}}^2\, \mathbf{x}. \tag{7}$$

For spherical satellites and assuming that the quantities A_{ref}, m, C_{D} and v_{rel} in Equation 7 have been precisely determined, the scale factor $f_{\text{s,SLR}}$ can be interpreted as a pure scaling of the thermospheric density ρ_{M} provided by a thermosphere model. In our numerical investigations, we apply in the sequel only the empirical thermosphere model NRLMSISE-00, which describes the neutral temperature and densities from the Earth surface to lower exosphere (0–1,000 km). The model possesses an extensive underlying database covering several decades, it is therefore driven by various data sets such as accelerometer and orbit-derived density data, inferred temperature from incoherent scatter radar, UV occultation measurements and the F10.7 index reflecting solar activity variations; for more details see Picone et al. (2002). As input, the model requires position and time as well as space weather data represented by the F10.7 and Kp index. NRLMSISE-00 takes statistical variability into account while interpolating, or extrapolating, the underlying data sets to estimate composition, temperature, and density for times, where geophysical conditions and locations are not covered by the database. Therefore, the NRLMSISE-00 model can be evaluated at any time and geographical position. An example output of thermospheric density as a function of altitude can be found in Figure 1.

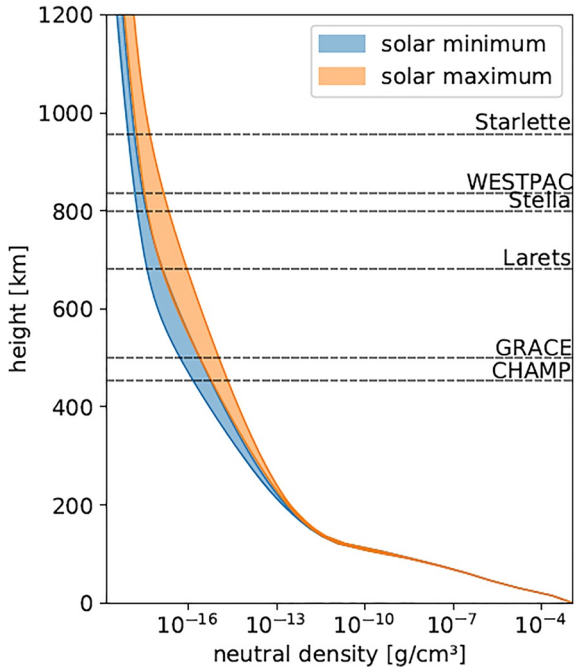

Figure 1. Exemplary sketch of the thermospheric density from the NRLMSISE-00 model as a function of altitude. For this, 72 altitude profiles were calculated along the equator. At a given time step, for solar maximum (January 01, 2003) and solar minimum (January 01, 2008), the minimum and maximum values at each altitude were determined. The black dashed lines show the mean altitudes of the used satellite missions.

To estimate a scale factor from SLR measurements according to Equations 6 and 7, a POD has to be performed. This way, a scale factor $f_{s,SLR}$ estimated with a time resolution of 24 up to 6 hr has to be interpreted as the mean value resulting from the integration along the orbit of the underlying time interval; see for example, Panzetta et al. (2018) and Rudenko et al. (2018). Within the scope of this study, the two software packages DOGS-OC and GROOPS are available to perform the POD. The results of these two packages are used to verify the reliability of the estimated scale factors (see Section 4.2). For such a validation, the same or at least a rather similar parameterization in both software packages is required; details on the software packages will be provided in the following two Sections 3.1.1 and 3.1.2. Satellite-specific information common to both software packages provided by the ILRS can be found at the ILRS webpage https://ilrs.cddis.eosdis.nasa.gov/missions/satellite_missions/index.html.

3.1.1. DGFI Orbit and Geodetic Parameter Estimation Software-Orbit Computation

At DGFI-TUM, the DGFI Orbit and Geodetic Parameter Estimation Software—DOGS (Bloβfeld, 2015; Gerstl, 1997) is used to process space geodetic observations like SLR, DORIS (Doppler Orbitography and Radiopositioning Integrated by Satellite), and VLBI (Very Long Baseline Interferometry) as well as their combination at various levels of the Gauss-Markov model. The orbit computation (OC) component of DOGS enables four modi, such as (1) orbit computation, (2) simulation of observations, (3) generation of normal equations, and (4) parameter correction. In this study, we use the last modus, where the numerical integration of a satellite orbit is performed together with adjusting a set of model parameters to the SLR observations applying an iterative least squares estimation. The analysis is based on commonly used geophysical background models (Petit & Luzum, 2010). The implemented integrator is based on a Gauss-Jackson predictor-corrector algorithm of seventh order with a typical step size between 5 and 60 s used for orbit integration (depending on the satellite altitude). For the comparison of the scale factors derived from the two SLR software packages, the same background models should be used in more or less the same way for the processing of Starlette, Stella, and Larets; see Table A1. In addition, the applied corrections to the observed SLR ranges are the tropospheric, relativistic, station-dependent, satellite-specific center of mass, and phase center corrections. The list of unknown parameters usually includes an initial state vector, SRP and ERP scale coefficients, thermospheric density scale factors, and empirical accelerations in along-track and normal directions. Furthermore, Earth rotation parameters, station coordinates, or range biases can be added. For the empirical accelerations, it is ensured that only negligible correlations with all estimated model scale factors occur. A detailed list of the estimated parameters of this study is given in Table A2.

According to Panzetta et al. (2018), the drag coefficient C_D in Equation 7 is computed analytically, based on physical principles described in a gas-surface interaction (GSI) model which is, in this study, the Sentman model (Sentman, 1961), where the accuracy is limited but current studies focus on the development of new GSI models, see for example, Mehta et al. (2017) and March et al. (2019), which are not considered here. When determining the C_D coefficient, the energy accommodation α is an important parameter that defines the momentum exchange of the gas molecules with the satellite surface. Based on the study of Pilinski (2011) and the assumption of a completely diffuse (cosine) reflection of the gas molecules, the energy accommodation coefficient $\alpha = 1$ (complete accommodation) can be chosen. Assuming that all variables in Equation 7 can be determined accurately, a POD procedure can be used to estimate the scale factors. As a compromise, we have chosen a temporal resolution of 12-hr for orbits of 7- and 15-day length. Up to the beginning of 1993, only 15-day orbits were computed for the Starlette satellite due to the small amount of observations during that time. For all other SLR satellite missions, 7-day orbits were computed. To compare scale factors derived from SLR and accelerometer measurements, we chose a different parameterization setup than in the comparison of the two POD software packages to increase the accuracy of the scale factors from SLR. In the POD procedures, additional parameters have been estimated, which are listed in Table A2. Scale factors of the following SLR satellite missions were estimated: Starlette, WESTPAC,

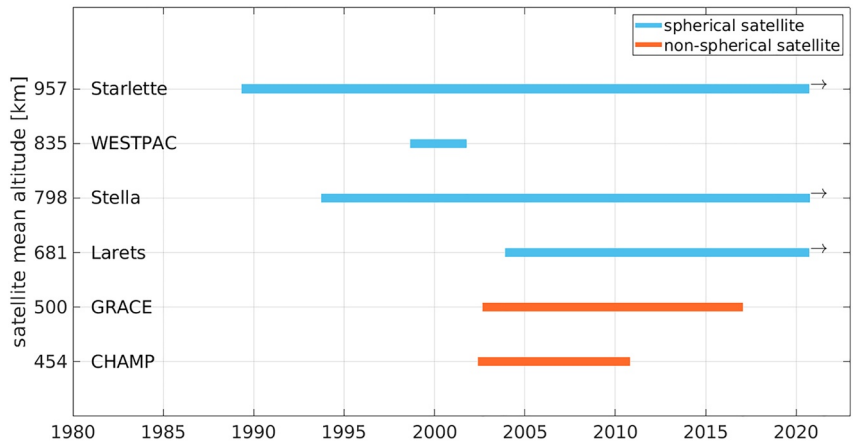

Figure 2. Mission lifetimes and mean altitudes of the satellite missions Starlette, WESTPAC, Stella, Larets, GRACE and CHAMP used in our study. An arrow indicates that the corresponding satellite is still in orbit and in use.

Stella and Larets. In addition to the thermosphere model NRLMSISE-00, the Horizontal Wind Model HWM14 (Drob et al., 2015) is used in both cases, which provides information about zonal and meridional winds in the atmosphere, see Equation 4.

For time intervals without any SLR observation, the scale factors are set to 1, since an estimation is not possible. More information on the applied approach, the processing, and a test of different satellites and empirical thermosphere models can be found in Panzetta et al. (2018) and Rudenko et al. (2018).

3.1.2. Gravity Recovery Object Oriented Programming System

The Gravity Recovery Object Oriented Programming System (GROOPS) was originally designed at the University of Bonn for gravity field recovery using data from the missions CHAMP and GRACE. While this area of work moved in 2010 to the Graz University of Technology, the further development of GROOPS in Bonn focused on satellite orbit determination from terrestrial tracking stations. The first mission evaluated by GROOPS was the lunar orbiter LRO, for which orbits with meter precision have been computed from radio and laser observations (Löcher & Kusche, 2018, 2019). Thereafter, the focus of research shifted to geodetic laser satellites. A recent outcome of this activity is a series of time-variable gravity fields derived from measurements to five SLR satellites (Löcher & Kusche, 2021).

The GROOPS software is a toolbox consisting of a number of individual programs; it is written in C++ and controlled by a graphical user interface. The module used for SLR analysis performs, like DOGS-OC, an iterative adjustment of the orbit parameters to minimize the observation residuals. This procedure strongly relies on numerical integration, which is carried out here by an Adams-Moulton integrator operated with a step size of 30 s. The stochastic modeling of the observations is based on the accuracies provided with the normal points from the ILRS. For data screening, a median-based procedure is applied. At a later stage, the data weighting is refined by variance component estimation following the approach of Förstner (1979). For this, the normal points are grouped by stations to balance the different noise levels of the laser systems.

For this study, data of three selected satellites, Starlette, Stella and Larets, were processed in orbits of 3 days length. As in the DOGS-OC computations, the scale factors for the thermospheric density were set up for periods of 12 hr each. The parametrization was otherwise chosen rather conservatively, for example, by not considering empirical forces. The observed ranges are corrected for the tropospheric and relativistic delays and the center-of-mass offsets of the satellites. Further station or satellite-dependent systematics are not considered but compensated for range biases set up on a monthly basis. The range corrections and the models applied in the orbit integration were mostly the same as those used in the DOGS-OC processing; the most substantial differences are the choice of the ocean tide model and a more recent model of the Earth's gravity field. For the drag coefficient, the Sentman model is applied, too. The drag itself, however, is slightly differently computed because a wind model is not applied in GROOPS. Comprehensive summaries of the used models and the parameter setup are provided in Tables A1 and A2.

3.2. Accelerometer

As mentioned before, space-borne accelerometry provides *in situ* thermospheric density data along the satellite orbit with a high temporal resolution of, for example, 10 s for GRACE. According to Equation 1, an accelerometer measures the non-gravitational acceleration acting on a spacecraft. Since the largest non-gravitational acceleration for LEO satellites is the atmospheric drag, there is a direct relation between the density at the position of the satellite and the measured acceleration. In this section, we briefly outline the processing of accelerometer measurements to derive thermospheric density values. The result will be used to obtain scale factors for the NRLMSISE-00 model in order to compare them to the SLR-derived scale factors in Section 4.1.

At first, accelerometer measurements have to be calibrated due to their measurement principle. Here, we apply the calibration parameters (daily biases and constant scale factors) as described in Vielberg et al. (2018), which were obtained within a POD. Gravitational background models used in the calibration are updated to the following versions: static gravity field GOCO06s (Kvas, Mayer-Gürr, et al., 2019), the time variable gravity field ITSG2018 (Kvas, Behzadpour, et al., 2019), the atmosphere and ocean de-aliasing product AOD1B RL06 (Dobslaw et al., 2017), and finally the ocean tide model FES 2014b (Carrère et al., 2015).

From the calibrated accelerometer measurements $\mathbf{a}_{\text{cal}}$, we solve for the aerodynamic acceleration

$$\mathbf{a}_{\text{aero}} = \mathbf{a}_{\text{cal}} - \mathbf{a}_{\text{srp}} - \mathbf{a}_{\text{erp}}. \tag{8}$$

The two accelerations $\mathbf{a}_{\text{srp}}$ and $\mathbf{a}_{\text{erp}}$, already introduced in Equation 2, are analytically modeled including the extensions suggested by Vielberg and Kusche (2020) accounting for thermal re-radiation at the satellite's surface and for the Earth's outgoing radiation from hourly CERES SYN1deg data (NASA/LARC/SD/ASDC, 2017) in combination with angular distribution models.

Finally, we derive thermospheric density values from the analytical relation in Equation 3 between the aerodynamic acceleration $\mathbf{a}_{\text{aero}}$ and the density ρ_{M}. After rearranging Equation 3 and solving for the density $\rho_{\text{M}} =: \rho_{\text{ACC}}$ we obtain under the consideration of Equation 8.

$$\rho_{\text{ACC}} := \frac{-2m \cdot \mathbf{x}^T \mathbf{a}_{\text{aero}}}{A \cdot \mathbf{x}^T \mathbf{c}_{\text{aero}} \cdot v_{\text{rel}}^2}. \tag{9}$$

As mentioned in the context of Equations 3 and 4, the scalar multiplication in Equation 9 with the unit vector $\mathbf{x}$ indicates the use of the along-track accelerations only. As in Vielberg et al. (2018), we apply the aerodynamic coefficient $\mathbf{c}_{\text{aero}}$ following Doornbos (2012) with an energy accommodation coefficient for GRACE of 0.93 and 0.85 for CHAMP. For the processing of accelerometer-derived densities, we use the GRACE Level-1B accelerometer data (ACC1B) together with reduced dynamic orbits (GNV1B; Case et al., 2010). For CHAMP, we apply Level 2 data as well as dynamic orbits (Prange, 2010; Prange et al., 2010). The resulting thermospheric density corresponds to the TND-IGG RL01 data set (Vielberg et al., 2021). Since this data set applies the NRLMSIS 2.0 model within the aerodynamic modeling, we modified the data for this study with the NRLMSISE-00 model.

Finally, the density according to Equation 9 can be used to adjust the density ρ_{M} of the empirical model to obtain the scale factor $f_{\text{s,ACC}}$ similar to $f_{\text{s,SLR}}$ introduced in Equation 7

$$f_{\text{s,ACC}} = \frac{\rho_{\text{ACC}}}{\rho_{\text{M}}}. \tag{10}$$

4. Analysis of the Results

In the following, we compare the scale factors $f_{\text{s,SLR}}$ and $f_{\text{s,ACC}}$ of the thermospheric density, obtained from SLR and accelerometer measurements for the six satellite missions shown in Figure 2.In a first comparison, we present thermospheric density scale factors derived from SLR measurements using the DOGS-OC software and from accelerometer measurements. For the latter, the scale factors are computed from on-board accelerometer data of CHAMP and GRACE. Here, the temporal resolution of the scale factors is fixed to 12 hr to allow the comparison with the SLR-derived scale factors using the same temporal resolution. The spherical SLR missions processed with DOGS-OC are Larets, Stella, WESTPAC, and Starlette, which are orbiting the Earth at different mean altitudes between 681 and 957 km (see Figure 2). Additionally, we compare our scale factors with fitted thermospheric density ratios (FDR) from the latest Emmert, Dhadly, and Segerman (2021) publication. The ratio

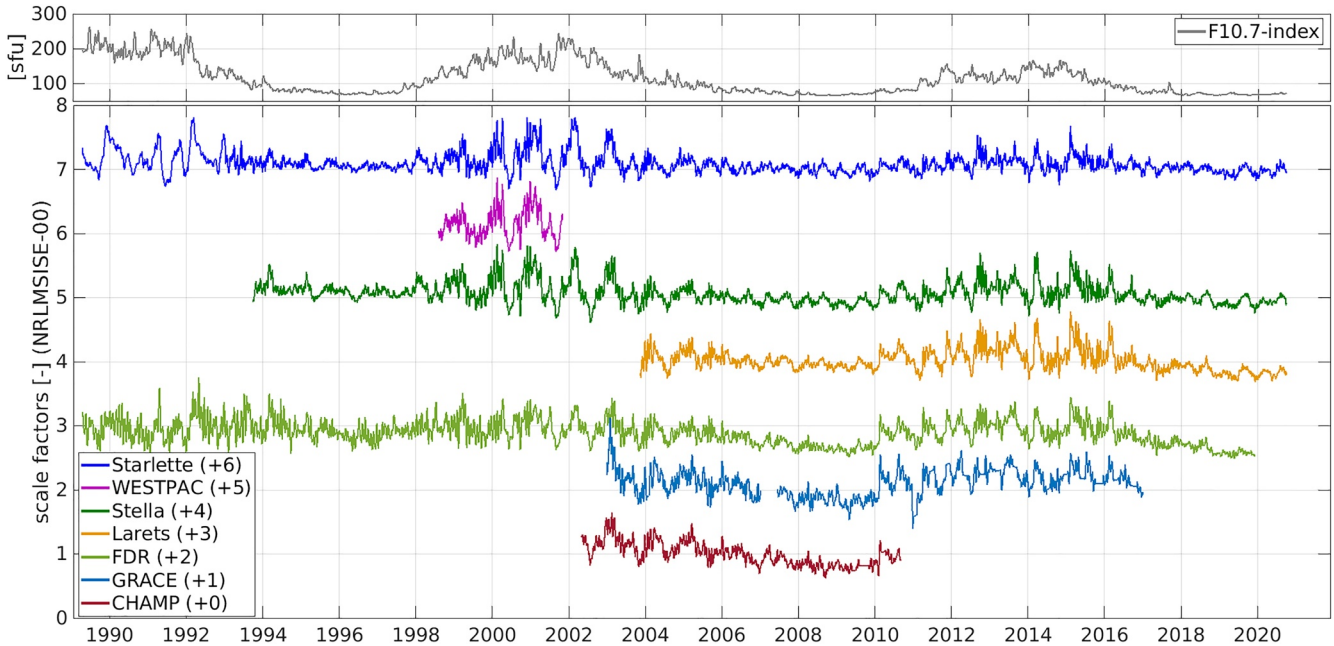

Figure 3. Time series of filtered scale factors $f_{s,SLR}$ of the thermospheric density from satellite laser ranging (using the DOGS-OC software), $f_{s,ACC}$ of the accelerometer measurements and of the fitted density ratios f_{FDR} in an averaged altitude of 575 km by Emmert, Dhadly, and Segerman (2021) (bottom) compared to the F10.7 solar activity index (top). The scale factor time series are shifted against each other by +1 according to their mean altitude to make them more distinguishable.

values "f_{FDR}" are comparable to our estimated scale factors, since both the ratios and scale factors are used to scale the modeled thermospheric density provided by the NRLMSISE-00 model. For the comparison, we used the orbit-derived density ratios over a time period from 1989 to 2019 at an averaged altitude of 575 km being the largest possible altitude of the FDR data set. The FDRs are derived from ~7,700 objects in low Earth orbits, for more details see Emmert, Dhadly, and Segerman (2021). The underlying data set has a temporal resolution of typically 3–4 days. For better readability, we refer only to "scale factors" in the following. Second, within the POD of the spherical satellites Larets, Stella and Starlette, scale factors with a temporal resolution of 12 hr using the SLR software packages DOGS-OC and GROOPS are estimated to assess their reliability and quality.

4.1. Comparison of SLR and Accelerometer-Derived Scale Factors

Figure 3 shows the estimated scale factors $f_{s,SLR}$, $f_{s,ACC}$, and f_{FDR} which were filtered by a 10-day moving average filter to remove noise. Only the GRACE time series suffers from a gap, namely between January and June 2007 when no data were provided.

To establish a relation between a space weather index and the filtered scale factor time series, the latter are plotted in Figure 3 against the time series of the 10-day averaged F10.7 index. It is probably the most widely used solar index, reflecting the solar extreme ultraviolet (EUV) irradiance at a frequency of 2.8 GHz, corresponding to a wavelength of 10.7 cm (Tapping, 2013). It serves as an input for the NRLMSISE-00 model and is a useful indicator of the solar activity because of its correlation with the number of sunspots. On time scales that are relevant for thermosphere studies, the solar EUV irradiance spectrum is generally dominated by the 27-day Sun rotation and the 11-year solar cycle. The latter can be clearly seen in Figure 3, where a solar maximum is reached approximately every 11–13 years (the last solar maximum have been identified at Nov. 1989, Nov. 2001, and April 2014), characterized by F10.7 values larger than 100 sfu (solar flux unit; 1 sfu = $10^{-22}\,\frac{\mathrm{W}}{\mathrm{m}^2\cdot\mathrm{Hz}}$). A similar behavior is also shown by the scale factor time series. Thereby, high solar activity is manifested in larger variations of the scale factors, whereas low solar activity is characterized by smaller variations of the scale factors. It can also be seen that our scale factors derived from SLR and accelerometer data agree well with the FDR scale factors. Hereby, it can be noticed that the FDR scale factors show a smoother variability compared to our data set. This might be caused by the fact that Emmert, Dhadly, and Segerman (2021) use an average altitude of 575 km whereas our derived scale factors are obtained at distinct altitudes of the respective satellites (cf. Figure 2). In addition, a

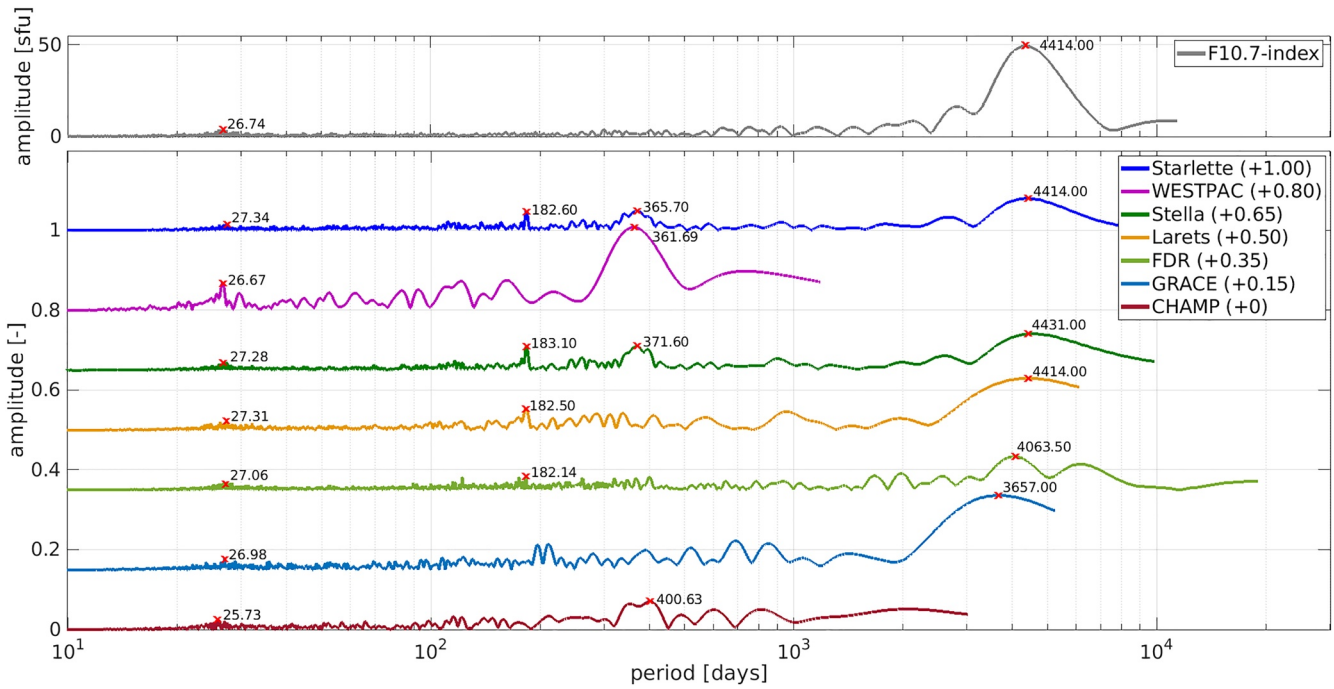

Figure 4. Discrete Fourier transform (DFT) amplitude spectrum of the space weather index F10.7 (top) and the scale factor time series of the selected satellite missions and the fitted thermospheric density ratios (FDR) data set by Emmert, Dhadly, and Segerman (2021) (bottom). The most dominant periods are marked with a red cross and the corresponding time period values in days. The spectra of the scale factor time series are shifted by 0.15, in case of FDR and Starlette by 0.20, corresponding to their mean altitude to make them more distinguishable.

systematic linear decrease of the FDR scale factors after 2016 is visible in the time series. This decrease is less prominent in the Starlette-, Stella-, and Larets-derived time series. The reason for this systematic difference is not yet clear as unfortunately, other time series like that one derived from GRACE accelerometer measurements ends before this time period.

Furthermore, the analysis of the discrete Fourier transform (DFT) amplitude spectra of the scale factor time series shown in Figure 4 indicate that the annual period and its harmonics as well as the solar cycle period are present. The 27-day solar rotation period can be clearly identified in all time series. For time series longer than 20 years, the 11-year solar cycle is visible. Especially the SLR-derived time series show seasonal periods comprising an annual and semi-annual signal. An semi-annual signal can also be identified in the spectrum of the FDR scale factors. In addition, some periods appear which cannot be explained yet and require further investigations. Moreover, it was tested if the scale factors are influenced by atmospheric gravity waves. Since these depend on local time as well as solar and magnetic activity, distinct peaks in the spectra shown in Figure 4 might be caused. To test this assumption, we assumed a gravity wave with a period of 9 hr, resulting in an alias period of approximately 1.5 days. From Figure 4, we can state that neither the spectrum of GRACE nor the CHAMP spectrum shows such peaks. Furthermore, studies revealed that gravity waves usually propagate only up to an altitude of around 500 km, so it is not likely to detect gravity waves in the spectra of the SLR satellites. For the WESTPAC satellite, Figure 4 shows a noisier spectrum compared to all other SLR satellites (many peaks between 30 and 180 days). This fact might be explained by the much shorter mission duration compared to the other SLR satellites. Taking a closer look to the magnitude of the scale factor variations, it is noticeable that they are smaller during low solar activity and vary of about 30% around the value 1, which is an indication that the thermosphere model NRLMSISE-00 reflects the thermospheric density sufficiently well. In contrast, during high solar activity, the scale factors are partly varying dramatically, for example, for Starlette they differ by up to 70% from the value 1 during solar maximum epochs. In general, the estimated scale factors indicate to which extent the thermospheric density calculated by the NRLMSISE-00 model must be adjusted to represent the density derived from the two measurement techniques. Therefore, it can be concluded that during high solar activity the NRLMSISE-00 model does not accurately represent the thermospheric density. Since the model underestimates and overestimates the density, respectively, it can be scaled by the factors estimated from the two geodetic observation techniques used here

Table 1
Mean Values and Standard Deviations (STD) of the Estimated Scale Factors $f_{s,SLR}$ and $f_{s,ACC}$ for Various Satellite Altitudes From Satellite Laser Ranging Measurements and From GRACE and CHAMP Accelerometer Measurements, Respectively

Solar activity	Statistics	Starlette	Stella	Larets	FDR	GRACE	CHAMP
Low	Mean	1.01	0.96	0.99	0.74	0.95	0.89
	STD	0.07	0.08	0.09	0.12	0.16	0.11
High	Mean	1.10	1.12	1.12	0.96	1.20	-
	STD	0.12	0.17	0.19	0.16	0.16	-

Note. In addition, the same quantities are given for the scale factors f_{FDR} by Emmert, Dhadly, and Segerman (2021) at the average altitude of 575 km. All values refer to low (January 01 2006–September 03, 2010) and high (January 01, 2011–December 31, 2016) solar activity conditions.

in this study. To investigate this topic further, Table 1 lists the mean values and standard deviations for selected scale factor time series, first for low solar activity (January 01, 2006–September 03, 2010) and second for high solar activity (January 01, 2011–December 31, 2016). Considering the mean values of the estimated scale factors for the different satellites, it is noticeable that they are close to 1. When the solar activity is low, the scale factors increase in general with increasing satellite altitude, whereas during high solar activity, the scale factors decrease with increasing altitude. Hence, on average, the NRLMSISE-00 model overestimates the thermospheric density at low solar activity and must be downscaled using the estimated scale factors, while the model underestimates the thermospheric density at high solar activity and must be upscaled. We notice that the mean values of the FDR scale factors show smaller values compared to our estimated scale factor time series. An offset of about 0.2 for both solar activity periods discussed above might be caused by the combination of objects for fitting the density ratios to gridded global average values. Additionally, a different model-dependent ballistic coefficient calculation was used by Emmert, Dhadly, and Segerman (2021). Compared to (Emmert, 2009) the ballistic coefficient for the primary reference object (Starshine 1) is about 8% higher. This might result in an overall decrease of the thermospheric density scale factors of about 8%. We also find a linear decrease of the thermospheric density scale factors from satellite missions above 680 km of about −5% per decade due to climate change. This fits well to the results from Solomon et al. (2015).

Table 2 shows the correlation coefficients between the different satellite solutions and the external data set of Emmert, Dhadly, and Segerman (2021). These values are computed at overlapping time intervals for each pair of the scale factor time series. They vary from 0.70 to almost 1. Three correlation coefficients, highlighted in bold in Table 2, will be pointed out in more detail in the following as they show the highest correlation: (1) a pure SLR comparison between WESTPAC and Stella: 0.98, (2) a mixed SLR and accelerometer solution between Larets and GRACE: 0.81, and (3) an accelerometer only solution between GRACE and CHAMP: 0.89. All three correlation coefficients show a value close to 1, indicating a high similarity of the time series. It is noticeable that the correlation coefficients become smaller with decreasing satellite altitude difference. The correlation coefficients

Table 2
Correlation Coefficients Between the Different Satellite Solutions and the External Data Set of Scale Factors by Emmert, Dhadly, and Segerman (2021)

	Starlette	WESTPAC	Stella	Larets	FDR	GRACE	CHAMP
Starlette	1	0.96	0.90	0.86	0.73	0.71	0.70
WESTPAC	0.96	1	0.98	-	0.83	-	-
Stella	0.90	**0.98**	1	0.93	0.84	0.77	0.75
Larets	0.86	-	0.93	1	0.93	0.81	0.74
FDR	0.73	0.83	0.84	0.93	1	0.89	0.92
GRACE	0.71	-	0.77	**0.81**	0.89	1	0.89
CHAMP	0.70	-	0.75	0.74	0.92	**0.89**	1

Note. The highest pure SLR, pure accelerometer and mixed SLR-accelerometer correlation coefficients from the various comparisons are highlighted in bold.

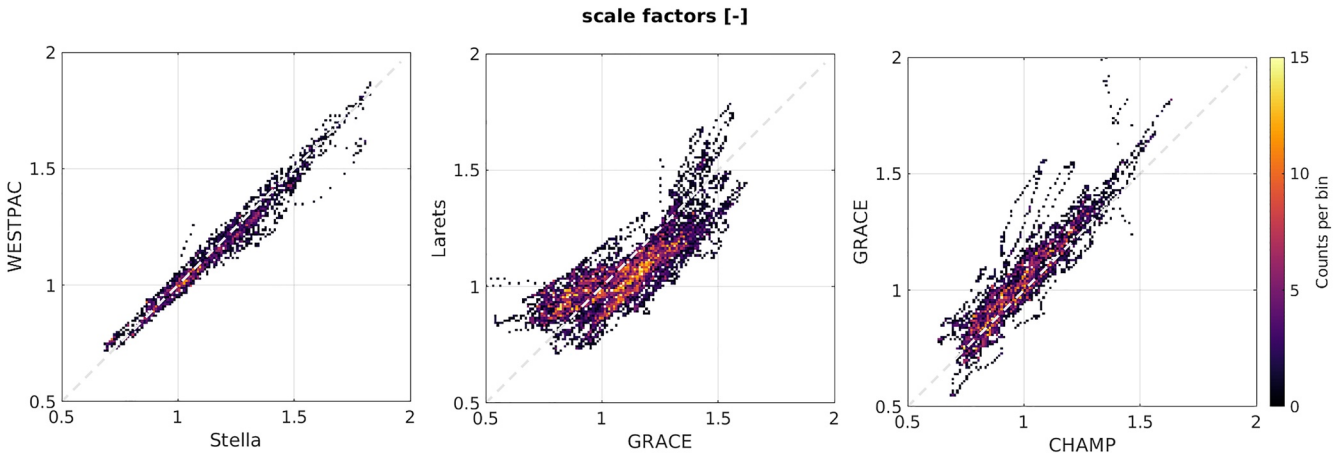

Figure 5. Scatter plots of the thermospheric density scale factors with the highest correlation coefficients highlighted in bold in Table 2. (left) Scale factors derived from satellite laser ranging (SLR) measurements only, (mid) scale factors from SLR and accelerometer, (right) scale factors from accelerometer measurements only.

of the FDR scale factors confirm a high agreement with our derived scale factor time series. Again, the correlation coefficients become smaller with decreasing altitude difference. The highest agreement is with the Larets scale factor time series with a value of 0.93 and the CHAMP time series with a value of 0.92.

An alternative analysis to identify the similarity of the time series is given by the corresponding scatter plots of the estimated scale factors for selected satellite missions as shown in Figure 5. The figure provides more insight into the different approaches for the estimation of the thermospheric density scale factors. For this purpose, we use the scale factor time series for the highest correlation coefficients highlighted in bold in Table 2. The scatter plots are created by plotting the corresponding time series against each other. The occurrence of the scale factors with time is counted and stored in bins. A bin was chosen with a size of 0.01 by 0.01. The scatter plots allow to quantify scale differences or offsets in the underlying scale factor time series. For a perfect match of the scale factors, the estimated scale factors of the different satellite solutions would be positioned on the dashed central diagonal. On the left side of Figure 5, a pure SLR comparison between the spherical satellites Stella and WESTPAC has been performed. The scale factors show a linear distribution, which indicates a high similarity of the two time series. This also confirms the previously determined high correlation coefficient between the Stella and the WESTPAC solution. In the mid panel of Figure 5, the derived scale factors from SLR and accelerometer observations are plotted with respect to each other. The scale factors reveal that for both methods scale factors of the thermospheric density are predominantly estimated close to 1. The distribution of the scale factors displays a noticeable scatter, a wider band around the dashed line, which is related to the smaller correlation coefficient of 0.81. In general, most counts of the scale factors per bin are located below the dashed line, which suggests that on average higher scale factors are determined with GRACE than with the SLR solution of Larets. A possible explanation could be that the thermospheric density provided by the NRLMSISE-00 model fits better to observations in the altitude range (681 km) of Larets than in the altitude range (500 km) of GRACE. On the right side, Figure 5 illustrates the comparison of the accelerometer-only solutions. Again, there is a scatter of the scale factors around the dashed line, verifying that they have a high degree of similarity disturbed only by a few outliers.

4.2. Comparison of SLR-Derived Scale Factors

The focus of this comparison is based on the analysis of the estimated scale factor time series for the thermospheric density derived from SLR measurements but using the two software packages DOGS-OC and GROOPS introduced in Sections 3.1.1 and 3.1.2. The parameterization for the PODs was selected as similar as possible (cf. Tables A1 and A2). Figure 6 shows the two estimated scale factor $f_{s,SLR}$ time series using DOGS-OC (blue) and GROOPS (orange), respectively, where again a 10-day moving average filter was applied to remove noise; statistical details are provided in Table 3. Again, considering the mean values of the estimated scale factors for the different satellites, it is noticeable that they are all close to 1. The least scaled time series are obtained using the measurements to Larets, where the mean values are 1.02 from DOGS-OC and 1.03 from GROOPS, see Table 3. In fact, the estimated scale factors of both POD software packages agree very well. The calculation of the

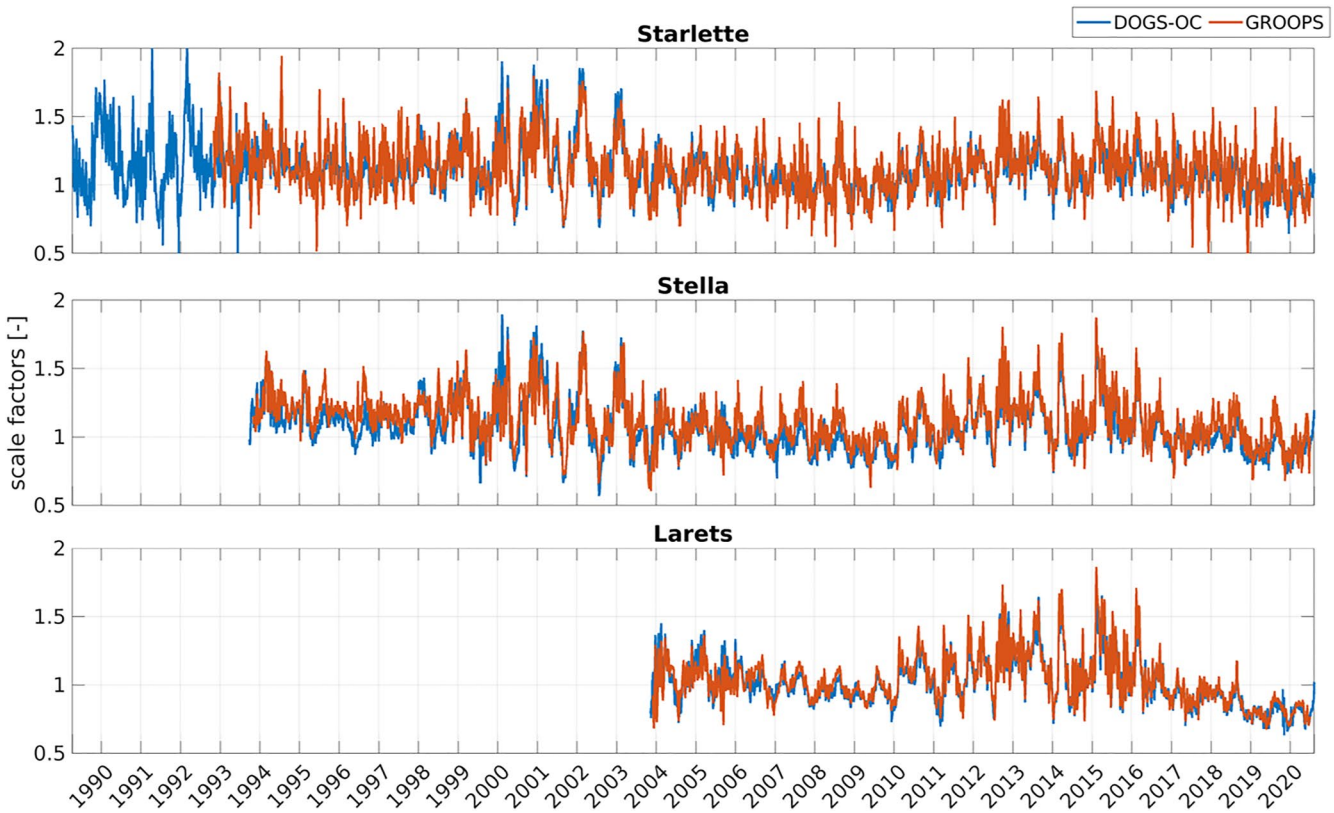

Figure 6. Filtered thermospheric density scale factors $f_{s,SLR}$ for Starlette, Stella, and Larets estimated from DOGS-OC (blue) and from GROOPS (orange).

correlation coefficient reveals a value of 0.94 for Larets and a significantly smaller value of 0.76 for Starlette. It will be stated here and discussed at the end of this Section, that (see Figure 2), the correlation coefficient and, thus, the similarity of the time series decreases with increasing satellite altitude. In Figure 7, scatter plots are again used to evaluate the similarity of the scale factor time series from the two software packages for the selected satellite missions. As before, the bin size was set to 0.01 by 0.01. The dashed line shows again the solution, where the scale factors of DOGS-OC and GROOPS perfectly match each other. The representation of the scale factors of Starlette shows a wide distribution compared to the other satellite solutions. The highest count of scale factors is located between 0.9 to 1.2, which also fits well with the determined mean values for DOGS-OC and GROOPS. However, the resulting scale factors for Stella are less scattered. The most counts per bin are in a range of 0.8–1.2. The best-fit is again obtained for the scale factors estimated from Larets measurements, where the most scale factors appear between 0.7 to 1.1. The analysis of the scatter plots discloses minor differences between scale factors of the various satellite solutions whereby the comparison between the software packages leads to rather similar results, which was expected, since similar background models were used. In tendency, DOGS-OC provides smaller scale factors of the thermospheric density compared to GROOPS, which is recognizable by the slight offset of the elevated number of scale factors per bin (colored in orange to light yellow) from the solution where DOGS-OC and GROOPS would perfectly match each other. Considering the corresponding satellite altitudes, it is noticeable that both Starlette and Stella are flying at altitudes of around 950 and 800 km, where the influence of the thermospheric density decreases (Figure 1). Consequently, other accelerations such as $\mathbf{a}_{srp}$ caused by SRP (cf. Equation 2) can become more important.

Table 3
Mean Value, Standard Deviation (STD) and Correlation Coefficient of the Estimated Scale Factors $f_{s,SLR}$ for Starlette, Stella, and Larets Computed With DOGS-OC and GROOPS

Satellite	Mean $f_{s,SLR}$ (DOGS-OC)	Mean $f_{s,SLR}$ (GROOPS)	STD (DOGS-OC)	STD (GROOPS)	correlation coefficient
Starlette	1.11	1.12	0.18	0.18	0.76
Stella	1.07	1.11	0.18	0.18	0.89
Larets	1.02	1.03	0.18	0.18	0.94

In contrast, Larets, which is orbiting the Earth at a mean altitude of around 680 km, is significantly more affected by the atmospheric drag. This is also the reason why the correlation coefficients in the right column of Table 3

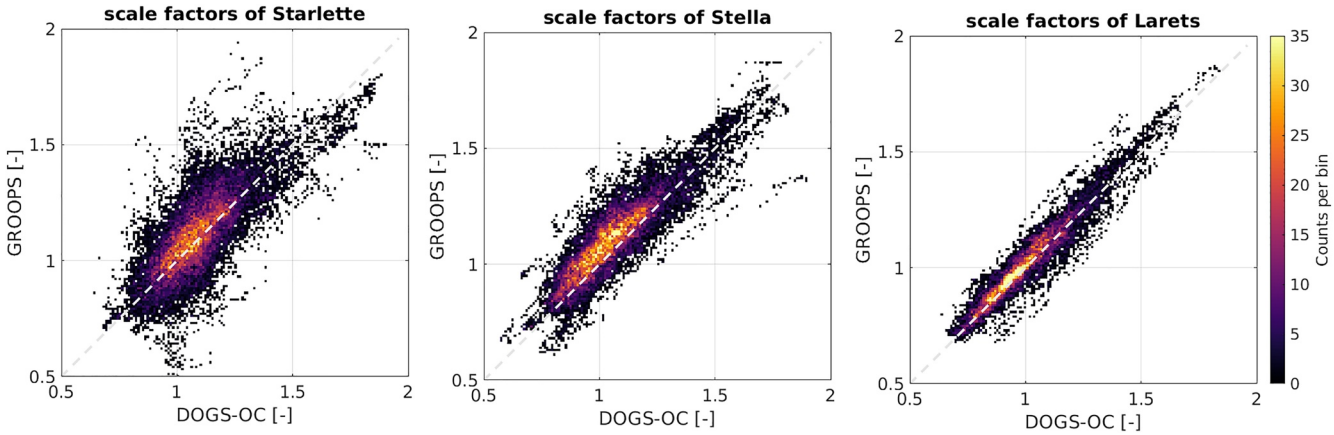

Figure 7. Scatter plots of thermospheric density scale factors $f_{s,SLR}$ for the three spherical satellites Starlette (left), Stella (mid), and Larets (right) calculated by the software packages DOGS-OC and GROOPS. The dashed line indicates the solution where the scale factors of DOGS-OC perfectly match those of GROOPS.

increases with decreasing satellite altitude. The stronger the thermospheric drag $\mathbf{a}_D$ as defined in Equation 7 appears in the SLR observation Equation 6, the more reliable the scale factor $f_{s,SLR}$ is estimable by means of the selected parameter estimation procedure. Consequently, the two SLR software packages DOGS-OC and GROOPS are providing rather similar results for Larets, since the parameter estimation procedures and the software parametrizations are fitting well to each other. With 0.89 the correlation coefficient for Stella is still high, but less as for Larets with 0.94.

5. Discussion and Outlook

This study underlines the importance of estimating scale factors for thermospheric densities from empirical thermosphere models, such as NRLMSISE-00, using geodetic observation techniques. When comparing the scale factors estimated from SLR and accelerometer measurements, we have demonstrated that they are rather similar and varying around the desired value 1, but showing deviations of up to 30% at low solar activity and up 70% at high solar activity. Thus, NRLMSISE-00 does not model the thermospheric density accurately enough during high solar activity, manifested in significant oscillations of the obtained scale factors. A comparison with scale factors from an external data set by Emmert, Dhadly, and Segerman (2021) show a general agreement with our SLR- and accelerometer-derived scale factor time series although the external scale factor time series seems to be smoother due to the use of an averaged altitude. This finding further supports the evaluation of the reliability of our derived SLR- and accelerometer-based thermospheric density scale factors.

To test the reliability of the scale factors determined from SLR measurements, the two independent POD software packages DOGS-OC from DGFI-TUM and GROOPS from IGG Bonn were used. We obtained the best agreement with measurements according to Larets with a correlation coefficient of 0.94. Overall, it can be seen that the solutions have larger correlation coefficients with decreasing altitude, which is related to the influence of the thermosphere and its exponential decrease with altitude. In this context we could state, that the estimated scale factor time series derived from the two software packages show quite similar results, although slightly different setups were used for the respective PODs.

Regarding the title of the study, the mid panel of Figure 5 might include the most important conclusion, since it compares the estimated scale factor $f_{s,ACC}$ from GRACE accelerometer measurements with the corresponding scale factors $f_{s,SLR}$ from SLR measurements to Larets. Since we compare here *in situ* information along the GRACE orbits with results which needs to be interpreted as mean values derived from the integration along the Larets orbit over an time interval of 12 hr, we cannot expect a linear behavior in the scatter plot as shown, for example, in the left panel of Figure 5. Besides the two rather different measurement techniques accelerometry and SLR as well as the two evaluation principles, we also have to take into account that $f_{s,ACC}$ and $f_{s,SLR}$ are determined from GRACE at a mean altitude of 500 km and Larets at a mean orbit height of 680 km. Consequently, and considering finally the right panel of Figure 5, our results are promising and allow not only a comparison of the scale factors from accelerometry and SLR, but also their combination. Such an application goes, however,

beyond the scope of this paper and will not be discussed here. Instead, we continue the interpretation of the mid panel of Figure 5. An offset of the highest count of scale factors below this solution is an evidence that larger scale factors are estimated with GRACE than with Larets, which can be, for example, by the fact that the thermospheric density provided by the NRLMSISE-00 model fits better in the altitude range of Larets than in the altitude range of GRACE as already stated before. It should also be mentioned that applying accelerometer-derived densities from other processing centers (Doornbos, 2012; Mehta et al., 2017) might lead to slightly different scale factors due to small biases between the density data sets, which are related to differences in the density processing, for example, macro-models, GSI models or radiation pressure force models.

To further our research, we will consider other SLR satellite missions, for example, GFZ-1, ANDE-C/P to get more information about the state of the thermosphere. It would also be interesting to study scale factors derived with respect to other empirical models and compare them with our results obtained in this study. Also, the scale factors can be improved by extending the GSI models. At present, the poor coverage of SLR tracking stations is improved by installing new SLR stations for example, in Ny-Ålesund (Norway) or Ponmundi (India) (Pearlman et al., 2019). Several simulation studies have been performed in the last time to extend the global SLR tracking network to achieve the objectives of the Global Geodetic Observing System (GGOS) and future terrestrial reference frames (Kehm et al., 2019). Thus, a significant improvement of SLR input data coverage for thermospheric density studies will be obtained.

Appendix A1: Additional Tables

Appendix A1.1: Background Models for the Processing of Spherical LEO Satellites

Table A1 shows different background models used in the two different POD software packages DOGS-OC and GROOPS are provided.

Table A1
The Following Models Have Been Used for the Processing of Spherical LEO Satellites With DOGS-OC and GROOPS

Forces	Model used in DOGS-OC	Model used in GROOPS
Earth gravity field	EIGEN-6S model (Förste et al., 2011). Static part: up to degree/order 120. Time variable part: up to degree/order 50.	EIGEN-6S4 (Förste et al., 2016). Static part: up to degree/order 120. Time variable part: up to degree/order 60.
Lunar gravity field	Up to degree/order 50 (Konopliv et al., 2001)	-
Short-term mass variations	-	AOD1B RL 06 (Dobslaw et al., 2017)
Solid Earth tides	International Earth Rotation and Reference Systems Service (IERS) Conventions 2010	IERS Conventions 2010
Ocean tides	EOT11a model (Savcenko & Bosch, 2012) up to degree/order 30 + 62 admittance waves (Petit & Luzum, 2010)	FES2014b (Carrère et al., 2016) up to degree/order 180 + admittance waves
Atmospheric tides	BB2003 (Biancale & Bode, 2006)	AOD1B RL 06
Ocean pole tide	(Desai, 2002)	(Desai, 2002)
Solid Earth pole tide	IERS Conventions 2010	IERS Conventions 2010
Permanent tides	IERS Conventions 2010	IERS Conventions 2010
General relativistic correction	Schwarzschild, de Sitter, Lense-Thirring (IERS Conventions 2010)	Schwarzschild, de Sitter, Lense-Thirring (IERS Conventions 2010)
Third body effect (direct tides)	DE-421: Sun, Moon, Mercury, Venus, Mars, Jupiter, Saturn (Folkner et al., 2008)	DE-421: Sun, Moon, Planets
Solar radiation pressure (SRP)	Cannonball model, constant radiation with eclipse modeling	Cannonball model
Earth radiation pressure (ERP)	Albedo and infrared (Knocke et al., 1988)	Albedo and infrared (Knocke et al., 1988)
Atmospheric drag	NRLMSISE-00	NRLMSISE-00

Appendix A1.2: Detailed List of the Estimated Parameters During the POD Procedures

Table A2 shows the estimated unknown parameters for the different parameterization setups.

Table A2
Estimation of Unknown Parameters During POD Using DOGS-OC (2 and 3 Column) and GROOPS (4 and 5 Column)

Parametrization	Estimated parameters (DOGS-OC)	Temporal resolution (DOGS-OC)	Estimated parameters (GROOPS)	Temporal resolution (GROOPS)
Comparison Section 4.1	Initial state vector	One set per orbit solution (initial epoch)	-	-
	Solar radiation pressure scale coefficient (SRP)	One per orbit solution	-	-
	Albedo scale coefficient (ERP)	One per orbit solution	-	-
	Scale factors (for thermospheric density)	12-hr	-	-
	Range biases	One bias per passage	-	-
	Coefficients of the empirical acceleration (a-long track and normal)	12-hr	-	-
	Earth rotation parameters (X, Y pole, UT1-UTC)	One set per day	-	-
Comparison Section 4.2	Initial state vector	One set per orbit solution (initial epoch)	Initial state vector	One set per orbit solution
	Solar radiation pressure scale coefficient (SRP)	One per orbit solution	Solar radiation pressure scale coefficient (SRP) and Albedo scale coefficient (ERP)	One per month
	Albedo scale coefficient (ERP)	One per orbit solution	Station coordinates	One set per month for selected stations
	Scale factors (for thermospheric density)	12-hr	Scale factors (for thermospheric density)	12-hr
	Range biases	One bias per station per arc	Range biases	One per month per satellite and station

Data Availability Statement

The thermospheric density scale factor time series discussed in this study are openly available at Zenodo via https://doi.org/10.5281/zenodo.5341420 with the License Creative Commons Attribution 4.0 International.

Acknowledgments
The work described in this study was carried out within the project "Development of High-precision Thermosphere Models for Improving Precise Orbit Determination of Low-Earth-Orbiting Satellites (TIPOD)" funded by the German Research Foundation (DFG) through the Special Priority Program 1788 "Study of Earth system dynamics with a constellation of potential field missions." The authors thank the editor and two anonymous reviewers for their comments, which allowed to improve this paper significantly. This research was funded by the German Research Foundation (DFG), grant number SCHM 2433/13-1 and the Technical University of Munich (TUM) in the framework of the Open Access Publishing Program. Open access funding enabled and organized by Projekt DEAL.

References

Bartels, J., Heck, N. H., & Johnston, H. F. (1939). The three-hour-range index measuring geomagnetic activity. *Terrestrial Magnetism and Atmospheric Electricity*, *44*(4), 411–454. https://doi.org/10.1029/TE044i004p00411

Biancale, R., & Bode, A. (2006). *Mean annual and seasonal atmospheric tide models based on 3-hourly and 6-hourly ECMWF surface pressure data (Scientific Technical Report STR06/01)*. GeoForschungsZentrum (GFZ) Potsdam.

Bloßfeld, M. (2015). *The key role of Satellite Laser Ranging towards the integrated estimation of geometry, rotation and gravitational field of the Earth (PhD thesis)*. Deutsche Geodätische Kommission.

Bloßfeld, M., Rudenko, S., Kehm, A., Panafidina, N., Müller, H., Angermann, D., et al. (2018). Consistent estimation of geodetic parameters from SLR satellite constellation measurements. *Journal of Geodesy*, *92*(9), 1003–1021. https://doi.org/10.1007/s00190-018-1166-7

Bloßfeld, M., Zeitlhöfler, J., Rudenko, S., & Dettmering, D. (2020). Observation-based attitude realization for accurate Jason satellite orbits and its impact on geodetic and altimetry results. *Remote Sensing*, *12*(4). https://doi.org/10.3390/rs12040682

Bowman, B., Tobiska, W. K., Marcos, F., Huang, C., Lin, C., & Burke, W. (2008). A new empirical thermospheric density model JB2008 using new solar and geomagnetic indices. In *AIAA/AAS Astrodynamics Specialist Conference and Exhibit*. https://doi.org/10.2514/6.2008-6438

Bruinsma, S. (2015). The DTM-2013 thermosphere model. *Journal of Space Weather and Space Climate*, *5*(A1). https://doi.org/10.1051/swsc/2015001

Carrère, L., Lyard, F., Cancet, M., & Guillot, A. (2015). FES 2014, a new tidal model on the global ocean with enhanced accuracy in shallow seas and in the Arctic region. In *EGU General Assembly Conference Abstracts* (Vol. 17, pp. 5481).

Carrère, L., Lyard, F., Cancet, M., Guillot, A., & Picot, N. (2016). FES 2014, a new tidal model - validation results and perspectives for improvements. In *Proceedings of the ESA Living Planet Symposium 2016* (pp. 9–13).

Case, K., Kruizinga, G., & Wu, S. (2010). *GRACE Level 1B data product user handbook. Tech. Rep. JPL D-22027*. Jet Propulsion Laboratory.
De Wit, T. D., & Bruinsma, S. (2017). The 30 cm radio flux as a solar proxy for thermosphere density modelling. *Journal of Space Weather and Space Climate*, *7*, A9. https://doi.org/10.1051/swsc/2017008
Desai, S. D. (2002). Observing the pole tide with satellite altimetry. *Journal of Geophysical Research*, *107*(C11), 7. https://doi.org/10.1029/2001JC001224
Dobslaw, H., Bergmann-Wolf, I., Dill, R., Poropat, L., Thomas, M., Dahle, C., et al. (2017). A new high-resolution model of non-tidal atmosphere and ocean mass variability for de-aliasing of satellite gravity observations: AOD1B RL06. *Geophysical Journal International*, *211*(1), 263–269. https://doi.org/10.1093/gji/ggx302
Doornbos, E. (2012). *Thermospheric density and wind determination from satellite dynamics*. Springer. https://doi.org/10.1007/978-3-642-25129-0
Doornbos, E., Van Den Ijssel, J., Lühr, H., Forster, M., & Koppenwallner, G. (2010). Neutral density and crosswind determination from arbitrarily oriented multiaxis accelerometers on satellites. *Journal of Spacecraft and Rockets*, *47*(4), 580–589. https://doi.org/10.2514/1.48114
Drob, D. P., Emmert, J. T., Meriwether, J. W., Makela, J. J., Doornbos, E., Conde, M., et al. (2015). An update to the Horizontal Wind Model (HWM): The quiet time thermosphere. *Earth and Space Science*, *2*(7), 301–319. https://doi.org/10.1002/2014EA000089
Emmert, J. T. (2009). A long-term data set of globally averaged thermospheric total mass density. *Journal of Geophysical Research*, *114*(A6). https://doi.org/10.1029/2009JA014102
Emmert, J. T., Dhadly, M. S., & Segerman, A. M. (2021). A globally averaged thermospheric density data set derived from two-line orbital element sets and special perturbations state vectors. *Journal of Geophysical Research: Space Physics*, *126*(8), e2021JA029455. https://doi.org/10.1029/2021JA029455
Emmert, J. T., Drob, D. P., Picone, J. M., Siskind, D. E., Jones Jr, M., Mlynczak, M. G., et al. (2021). NRLMSIS 2.0: A whole-atmosphere empirical model of temperature and neutral species densities. *Earth and Space Science*, *8*(3). https://doi.org/10.1029/2020EA001321
Folkner, W. F., Williams, J. G., & Boggs, D. H. (2008). *Planetary ephemeris DE421 for Phoenix navigation*. JPL IOM 343R-08-002.
Förste, C., Bruinsma, S., Flechtner, F., Marty, J.-C., Dahle, C., Abrykosov, O., et al. (2011). *EIGEN-6 a new combined global gravity field model including GOCE data from the collaboration of GFZ Potsdam and GRGS-Toulouse*. EGU General Assembly.
Förste, C., Bruinsma, S., Abrikosov, O., Rudenko, S., Lemoine, J. M., Marty, J. C., et al. (2016). *EIGEN-6S4 A time-variable satellite-only gravity field model to d/o 300 based on LAGEOS, GRACE and GOCE data from the collaboration of GFZ Potsdam and GRGS Toulouse (Version 2)*. GFZ Data Services. https://doi.org/10.5880/icgem.2016.008
Förstner, W. (1979). Ein Verfahren zur Schätzung von Varianz- und Kovarianzkomponenten. *Allgemeine Vermessungsnachrichten*, (11–12), 446–453.
Gerstl, M. (1997). Parameterschätzung in DOGS-OC. In *DGFI Interner Bericht, MG/01/1996/DGFI* (2nd ed.) (in German).
Kehm, A., Bloßfeld, M., König, P., & Seitz, F. (2019). Future TRFs and GGOS–where to put the next SLR station? *Advances in Geosciences*, *50*, 17–25. https://doi.org/10.5194/adgeo-50-17-2019
Knocke, P., Ries, J., & Tapley, B. (1988). Earth radiation pressure effects on satellites. In *Astrodynamics conference* (p. 4292). https://doi.org/10.2514/6.1988-4292
Konopliv, A. S., Asmar, S. W., Carranza, E., Sjogren, W. L., & Yuan, D. N. (2001). Recent gravity models as a result of the Lunar Prospector mission. *Icarus*, *150*(1), 1–18. https://doi.org/10.1006/icar.2000.6573
Kvas, A., Behzadpour, S., Ellmer, M., Klinger, B., Strasser, S., Zehentner, N., & Mayer-Gürr, T. (2019). ITSG-Grace 2018: Overview and evaluation of a new GRACE-only gravity field time series. *Journal of Geophysical Research: Solid Earth*, *124*(8), 9332–9344. https://doi.org/10.1029/2019JB017415
Kvas, A., Mayer-Gürr, T., Krauss, S., Brockmann, J. M., Schubert, T., Schuh, W.-D., et al. (2019). *The satellite-only gravity field model GO-CO06s*. Data Publication. GFZ Data Services. https://doi.org/10.5880/ICGEM.2019.002
Lean, J. L., Picone, J. M., Emmert, J. T., & Moore, G. (2006). Thermospheric densities derived from spacecraft orbits: Application to the Starshine satellites. *Journal of Geophysical Research*, *111*(A4). https://doi.org/10.1029/2005JA011399
Löcher, A., & Kusche, J. (2018). Precise orbits of the Lunar Reconnaissance Orbiter from radiometric tracking data. *Journal of Geodesy*, *92*, 989–1001. https://doi.org/10.1007/s00190-018-1124-4
Löcher, A., & Kusche, J. (2019). Assessment of the impact of one-way laser ranging on orbit determination of the Lunar Reconnaissance Orbiter. *Journal of Geodesy*, *93*, 2421–2428. https://doi.org/10.1007/s00190-018-1200-9
Löcher, A., & Kusche, J. (2021). A hybrid approach for recovering high-resolution temporal gravity fields from satellite laser ranging. *Journal of Geodesy*, *95*(1), 1–15. https://doi.org/10.1007/s00190-020-01460-x
March, G., Visser, T., Visser, P. N. A. M., & Doornbos, E. N. (2019). CHAMP and GOCE thermospheric wind characterization with improved gas-surface interactions modelling. *Advances in Space Research*, *64*(6), 1225–1242. https://doi.org/10.1016/j.asr.2019.06.023
Matzka, J., Stolle, C., Yamazaki, Y., Bronkalla, O., & Morschhauser, A. (2021). The geomagnetic Kp index and derived indices of geomagnetic activity. *Space Weather*. https://doi.org/10.1029/2020SW002641
Mehta, P. M., Walker, A. C., Sutton, E. K., & Godinez, H. C. (2017). New density estimates derived using accelerometers on board the CHAMP and GRACE satellites. *Space Weather*, *15*(4), 558–576. https://doi.org/10.1002/2016SW001562
Montenbruck, O., & Gill, E. (2000). *Satellite orbits, models, methods and applications*. Springer. https://doi.org/10.1007/978-3-642-58351-3
NASA/LARC/SD/ASDC. (2017). *CERES and GEO-Enhanced TOA, Within-Atmosphere and Surface Fluxes, Clouds and Aerosols 1-Hourly Terra-Aqua Edition4A*. NASA Langley Atmospheric Science Data Center DAAC. https://doi.org/10.5067/TERRA+AQUA/CERES/SYN1DEG-1HOUR_L3.004A
Panzetta, F., Bloßfeld, M., Erdogan, E., Rudenko, S., Schmidt, M., & Müller, H. (2018). Towards thermospheric density estimation from SLR observations of LEO satellites: A case study with ANDE-Pollux satellite. *Journal of Geodesy*, *93*(3), 353–368. https://doi.org/10.1007/s00190-018-1165-8
Pearlman, M. R., Noll, C. E., Pavlis, E. C., Lemoine, F. G., Combrink, L., Degnan, J. J., et al. (2019). The ILRS: Approaching 20 years and planning for the future. *Journal of Geodesy*, *93*(11), 2161–2180. https://doi.org/10.1007/s00190-019-01241-1
Petit, G., & Luzum, B. (2010). *IERS conventions (2010) (tech. Rep.)*. Bureau International des Poids et Mesures (France).
Picone, J. M., Hedin, A. E., Drob, D. P., & Aikin, A. C. (2002). NRLMSISE-00 empirical model of the atmosphere: Statistical comparisons and scientific issues. *Journal of Geophysical Research*, *107*(A12), SIA–SI15. https://doi.org/10.1029/2002JA009430
Pilinski, M. D. (2011). *Dynamic gas-surface interaction modeling for satellite aerodynamic computations (PhD thesis)*. University of Colorado at Boulder.
Prange, L. (2010). *Global gravity field determination using the GPS measurements made onboard the low earth orbiting satellite CHAMP (PhD thesis)*. Institut für Geodäsie und Photogrammetrie, Geodätisch-geophysikalische Arbeiten in der Schweiz, Zürich.
Prange, L., Jäggi, A., Dach, R., Bock, H., Beutler, G., & Mervart, L. (2010). AIUB-CHAMP02S: The influence of GNSS model changes on gravity field recovery using spaceborne GPS. *Advances in Space Research*, *45*(2), 215–224. https://doi.org/10.1016/j.asr.2009.09.020

Qian, L., Burns, A. G., Emery, B. A., Foster, B., Lu, G., Maute, A., et al. (2014). The NCAR TIE-GCM: A community model of the coupled thermosphere/ionosphere system. *Modeling the Ionosphere-Thermosphere System*, *201*, 73–83. https://doi.org/10.1002/9781118704417.ch7

Rudenko, S., Neumayer, K.-H., Dettmering, D., Esselborn, S., Schöne, T., & Raimondo, J.-C. (2017). Improvements in precise orbits of altimetry satellites and their impact on mean sea level monitoring. *IEEE Transactions on Geoscience and Remote Sensing*, *55*(6), 3382–3395. https://doi.org/10.1109/TGRS.2017.2670061

Rudenko, S., Schmidt, M., Bloßfeld, M., Xiong, C., & Lühr, H. (2018). Calibration of empirical models of thermospheric density using satellite laser ranging observations to near-earth orbiting spherical satellites. In J. T. Freymueller & L. Sánchez (Eds.), *International symposium on advancing geodesy in a changing world* (Vol. 149, pp. 119–127). Springer International Publishing. https://doi.org/10.1007/1345_2018_40

Savcenko, R., & Bosch, W. (2012). *EOT11A-empirical ocean tide model from multi-mission satellite altimetry*. DGFI Report No. 89.

Sentman, L. H. (1961). *Free molecule flow theory and its application to the determination of aerodynamic forces (LMSC-448514)*. Lockheed Missiles Space Company.

Solomon, S. C., Qian, L., & Roble, R. G. (2015). New 3-D simulations of climate change in the thermosphere. *Journal of Geophysical Research: Space Physics*, *120*(3), 2183–2193. https://doi.org/10.1002/2014JA020886

Sutton, E. K., Nerem, R. S., & Forbes, J. M. (2007). Density and winds in the thermosphere deduced from accelerometer data. *Journal of Spacecraft and Rockets*, *44*(6), 1210–1219. https://doi.org/10.2514/1.28641

Tapping, K. (2013). The 10.7 cm solar radio flux (F10. 7). *Space Weather*, *11*(7), 394–406. https://doi.org/10.1002/swe.20064

Vielberg, K., Forootan, E., Lück, C., Löcher, A., Kusche, J., & Börger, K. (2018). Comparison of accelerometer data calibration methods used in thermospheric neutral density estimation. *Annales Geophysicae*, *36*(3), 761–779. https://doi.org/10.5194/angeo-36-761-2018

Vielberg, K., & Kusche, J. (2020). Extended forward and inverse modeling of radiation pressure accelerations for LEO satellites. *Journal of Geodesy*, *94*(4), 43. https://doi.org/10.1007/s00190-020-01368-6

Vielberg, K., Lück, C., Corbin, A., Forootan, E., Löcher, A., & Kusche, J. (2021). TND-IGG RL01: Thermospheric neutral density from accelerometer measurements of GRACE, CHAMP and Swarm [data set]. PANGAEA. Retrieved from https://doi.pangaea.de/10.1594/PANGAEA.931347

Viereck, R. A., & Puga, L. C. (1999). The NOAA Mg II core-to-wing solar index: Construction of a 20-year time series of chromospheric variability from multiple satellites. *Journal of Geophysical Research*, *104*(A5), 9995–10005. https://doi.org/10.1029/1998JA900163

Xiong, C., Lühr, H., Schmidt, M., Bloßfeld, M., & Rudenko, S. (2018). An empirical model of the thermospheric mass density derived from CHAMP satellite. *Annales Geophysicae*, *36*, 1141–1152. https://doi.org/10.5194/angeo-36-1141-2018